

Article

## End-Fire Antenna for BAN at 60 GHz: Impact of Bending, On-Body Performances, and Study of an On to Off-Body Scenario

Anda R. Guraliuc <sup>1,\*</sup>, Nacer Chahat <sup>2</sup>, Carole Leduc <sup>1</sup>, Maxim Zhadobov <sup>1</sup> and Ronan Sauleau <sup>1</sup>

<sup>1</sup> Institute of Electronics and Telecommunications of Rennes (IETR), UMR CNRS 6164, University of Rennes 1, Rennes 35700, France; E-Mails: carole.leduc@univ-rennes1.fr (C.L.); maxim.zhadobov@univ-rennes1.fr (M.Z.); ronan.sauleau@univ-rennes1.fr (R.S.)

<sup>2</sup> Jet Propulsion Laboratory (JPL), Pasadena, CA 91109, USA; E-Mail: nacer.e.chahat@jpl.nasa.gov

\* Author to whom correspondence should be addressed; E-Mail: anda.guraliuc@univ-rennes1.fr; Tel.: +33-2-2323-3786; Fax: +33-2-2323-6969.

Received: 28 February 2014; in revised form: 27 March 2014 / Accepted: 31 March 2014 /

Published: 8 April 2014

---

**Abstract:** A compact end-fire wearable Yagi-Uda antenna covering the entire 57–64 GHz frequency band is characterized in free space, in the presence of a skin-equivalent phantom and under bending conditions. The results demonstrate that, when placed on the body and/or bended, the antenna preserves satisfactory performances. The possibility of its use for an on/off-body communications at 60 GHz is investigated numerically and experimentally in a representative scenario in terms of *E*-field and power flow distributions, as well as in terms of path gain. It is shown that this antenna is a suitable candidate for high-data-rate short-range on/off-body transmissions.

**Keywords:** end-fire Yagi-Uda antenna; wearable antenna; millimeter waves; body area network; body-centric communications; propagation

---

### 1. Introduction

Recently, the unlicensed 57–64 GHz band has been identified as a highly promising solution for body area networks (BAN) [1] since it provides several advantages compared to microwave BAN [2]. Indeed, very high data rates can be reached (up to 5–7 Gb/s) [3] whilst providing high level of security

and low interference with adjacent networks [4]. Besides, the on-body devices are smaller at millimeter waves compared to those operating at microwaves.

Few studies have been reported so far in the literature on 60-GHz BAN communications. Propagation studies have shown that (1) 60-GHz BAN allows more BAN users to be co-located within a certain area [4] and (2) it is possible to establish a BAN with a reliable radio link and coverage [5]. Besides, a tissue-equivalent phantom emulating the dielectric properties of the human skin in the 55–65 GHz range has been proposed [6] for antenna measurements and propagation studies [7], [8]. Furthermore, the state of knowledge of the electromagnetic and thermal interactions of millimeter waves with the human body has been reviewed in [9].

Some 60-GHz antennas with end-fire radiation patterns have been recently designed [10], [11] for on-body communications. A piece of meat was used to mimic the human body and to study the impact of the body upon the antenna performance. In [12–14] wearable patch and Yagi-Uda antennas for on-body communications at 60 GHz have been introduced. In [12] it is shown that bending a patch antenna printed on a textile has small impact on the reflection coefficient and antenna gain. In [13] a textile Yagi-Uda antenna matched in the 57–64 GHz band with an end-fire radiation pattern is characterized in the presence of a flat skin-equivalent phantom, without considering the bending effect.

It is well known that in some BAN applications the antenna cannot be always kept flat, so the bending effect should be investigated and taken into account for possible applications. At microwaves, bending effect has been widely studied for different antenna types, such as patch antenna [15–18], planar inverted F-antenna (PIFA) [19], dual-band antenna printed on electromagnetic band gap structure (EBG) [20]. These studies showed that antenna impedance matching and radiation patterns are affected by bending. Furthermore, Ref. [19] shows that the textile antenna performance can be substantially affected when it is crumpled, with a significant frequency shift and degraded radiation patterns. On the other hand it is shown in [20] that a textile antenna integrated with an EBG surface is tolerant to the bending on the body. Some effects on the radiation pattern and resonant frequency are noted, although the bandwidth and antenna gain remains unchanged.

In this study, the wearable Yagi-Uda antenna operating in the 57–64 GHz range briefly introduced in [14] is characterized for the first time under bending conditions on a skin-equivalent phantom. Furthermore, the propagation is studied for a realistic communication scenario between this antenna placed on a human hand and an off-body antenna. In practice, the antenna could be integrated in a wristwatch, bracelet, or gloves for medical, military or entertainment applications where high-data-rate transmissions are needed.

This paper is organized as follows. The antenna design and its main characteristics in free space, in the presence of a skin-equivalent phantom and under bending conditions are presented in Section II. In addition, the *E*-field distribution in free space and around a homogeneous skin-equivalent model is numerically investigated. In Section III, the propagation is investigated for realistic on to off-body scenario. Finally, the conclusions are drawn in Section IV.

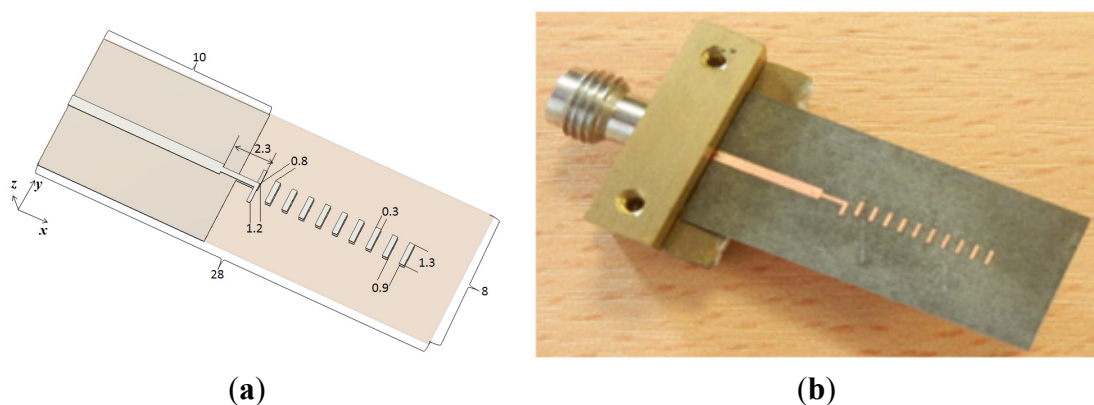
## 2. Antenna Model and Characteristics

### 2.1. Antenna Model

The compact wearable antenna used in this study was previously briefly introduced in [14]. Here for the first time the antenna characteristics are investigated under bending conditions both in free space and on a skin-equivalent phantom.

This low-profile high-gain ( $\sim 12$  dBi) antenna with an end-fire radiation is printed on a 0.254 mm-thick RT Duroid 5880 substrate ( $\epsilon_r = 2.2$ ,  $\tan\delta = 0.003$ ). The layout and the manufactured antenna are shown in Figure 1.

**Figure 1.** (a) CAD antenna view (dimensions are in mm); (b) Manufactured antenna with a V-connector.



### 2.2. Reflection Coefficient

The reflection coefficient ( $S_{11}$ ) of the antenna with V-connector (Figure 1b) is measured with a 110 GHz vector network analyzer (Agilent 8510XF) after performing an open-short-load (OSL) calibration.

Firstly, the  $S_{11}$  was measured in free space. As shown in Figure 2, both measured and simulated  $S_{11}$  are in good agreement and below  $-10$  dB in the whole 57–64 GHz range. For the numerical modeling CST Microwave Studio<sup>®</sup> has been used. The  $S_{11}$  was also measured when the antenna was placed on a semi-solid phantom emulating the dielectric properties of the human skin. The skin-equivalent phantom was prepared following the procedure presented in [21]. The antenna/body spacing ( $h$ ) is 5.6 mm (due to the connector presence); in this case the reflection coefficient remains almost the same as in free space within the whole frequency range.

Secondly, the  $S_{11}$  was measured under bending conditions (in  $H$ -plane), when the antenna is placed on a semi-cylindrical Rohacel HF51 foam and on a skin-equivalent phantom with a radius  $R = 15$  mm (Figure 3). The chosen radius represents a severe “worst case” test. As shown in Figure 2, the  $S_{11}$  remains below  $-10$  dB over the whole frequency range. These results demonstrate that despite the severe bending and the presence of the human body, the  $S_{11}$  remains below  $-10$  dB proving the robustness of the antenna performances in terms of reflection coefficient.

**Figure 2.** Reflection coefficient of the antenna in free space, under bending conditions on a semi-cylindrical foam and on a skin-equivalent phantom, and for the antenna placed on the phantom for the antenna/body spacing  $h = 5.6$  mm. [S]—Simulations, [M]—Measurements.

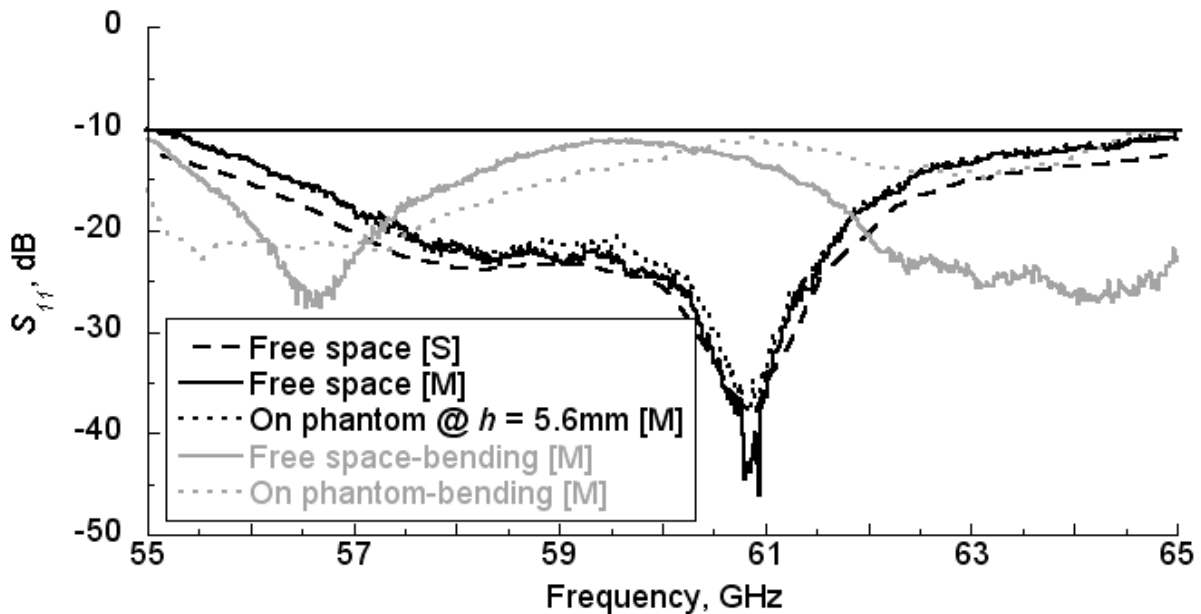
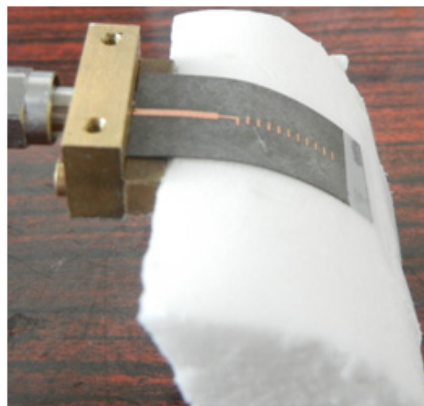


**Figure 3.** Bending antenna in  $H$ -plane on a semi-cylindrical skin-equivalent phantom with  $R = 15$  mm.



### 2.3. Radiation Patterns

The radiation patterns in free space for  $E$ - and  $H$ -planes (*i.e.*,  $xy$ -plane and  $xz$ -plane, respectively) are plotted in Figure 4. The simulated and measured radiation patterns at 60 GHz are in good agreement. Generally the cross-polarization remains lower than  $-10$  dB in both planes, except around  $30^\circ$  where a slight increase is noticed compared to the co-polarization component. At 60 GHz, the measured and computed gains equal 11.8 dBi and 12.1 dBi respectively. The antenna radiation efficiency (94.4%) calculated as the ratio between the measured gain and computed directivity is in good agreement with the simulated value (92.2%). Figure 5 shows the simulated radiation pattern in free space at 57–60–64 GHz. Results demonstrate stable antenna performances in the 57–64 GHz frequency range.

**Figure 4.** Measured and simulated radiation patterns in free space at 60 GHz: (a) *E*- and (b) *H*-planes.

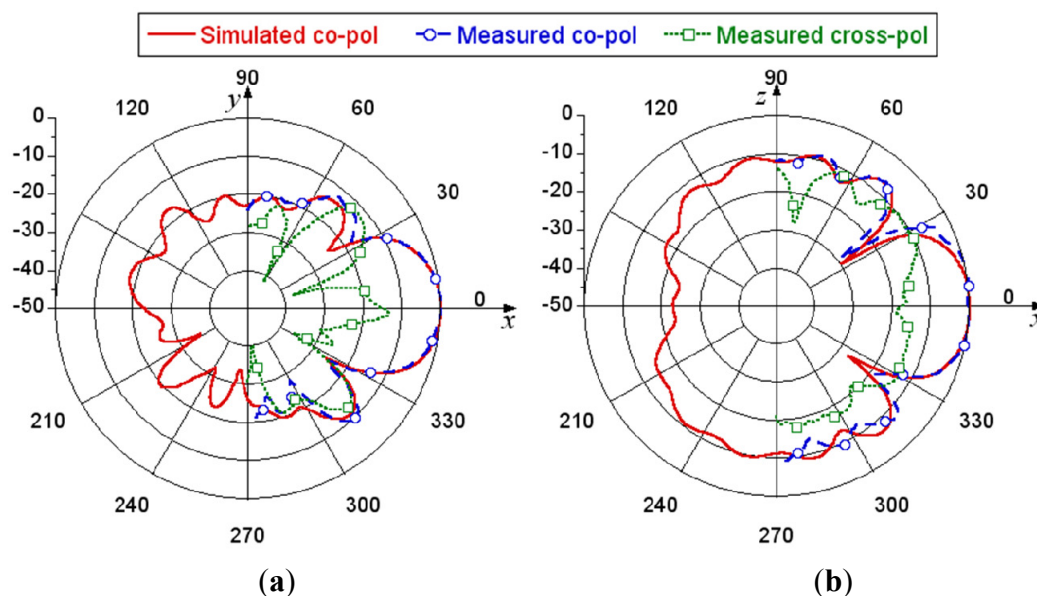
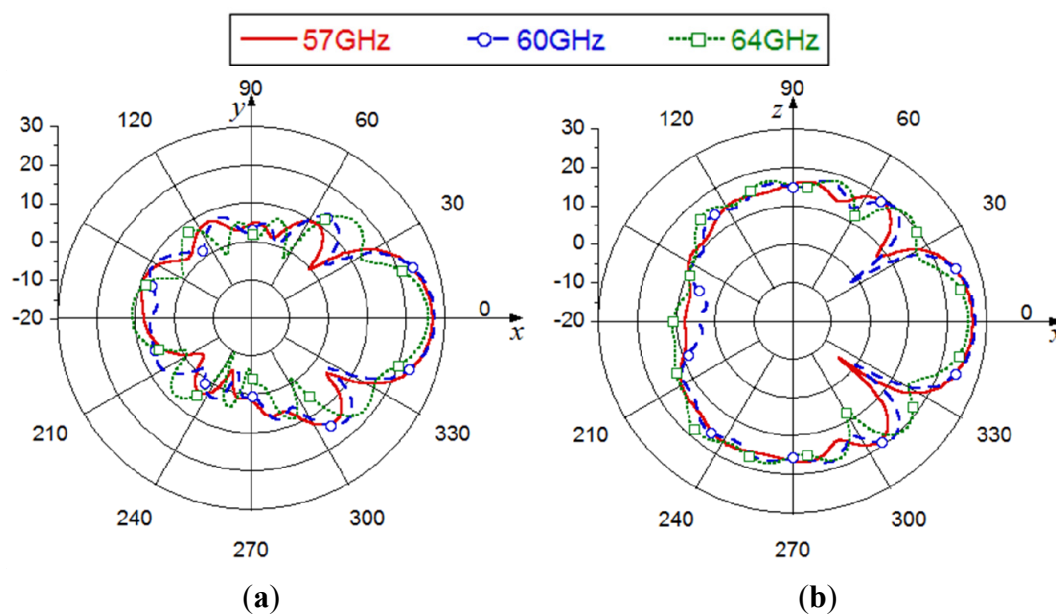


**Figure 5.** Simulated radiation patterns in free space at 57–60–64 GHz: (a) *E*- and (b) *H*-planes.



The measured radiation patterns in both *E* and *H* planes at 60 GHz of the antenna placed at a distance  $h = 5.6$  mm on a flat skin-equivalent phantom are shown in Figure 6. As it can be seen, both *E*- and *H*-planes are strongly affected by the human body presence because of reflection from and absorption in the body.

It was previously shown that, at microwaves, the antennas in the presence of the human body suffer from drastic decrease of efficiency and gain [22–26]. At 60 GHz, the radiation pattern in the *H*-plane is tilted (about  $10^\circ$ ) because of reflections occurring at the air/phantom interface. It is well known that the reflected power depends on the incidence angle and polarization, and for normal incidence 30%–40% of the incident power is reflected [9]. Indeed, due to the reflection on the skin phantom, the

gain increases by 3 dB when the antenna is on the phantom compared to the antenna in free space. The measured gain (15.2 dBi) is in good agreement with the computed one (15 dBi). Furthermore, compared to the free space configuration, back radiation is significantly reduced because of the absorption in the human body.

**Figure 6.** Measured and simulated radiation patterns of the antenna placed at a distance  $h = 5.6$  mm from the skin-equivalent phantom at 60 GHz: (a) *E*- and (b) *H*-planes.

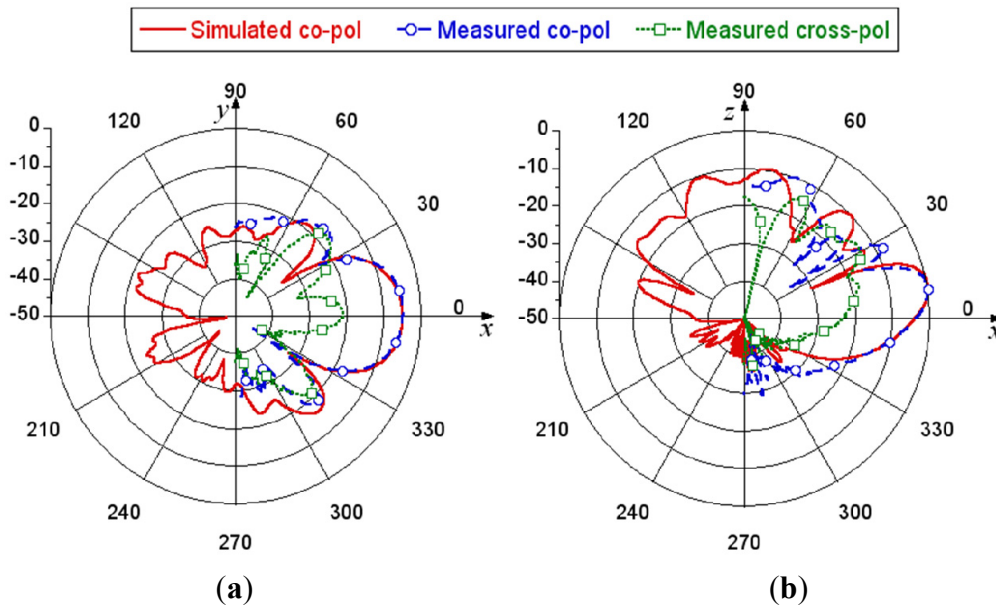
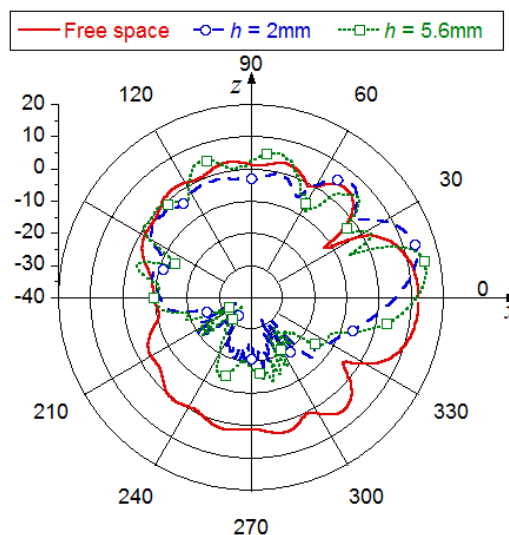


Figure 7 shows the computed gain for different antenna/phantom distances. An antenna gain increase is noticed when the antenna is placed above the phantom (3 dB for  $h = 5.6$  mm). It should be also noted that at  $h = 2$  mm the radiation pattern in the *H*-plane is tilted by  $20^\circ$ , while at 5.6 mm the tilt angle is  $10^\circ$ . In Table 1, a summary of the computed and measured gain is provided, as well as the simulated antenna radiation efficiency. It is shown that the efficiency decreases when the antenna/phantom distance decreases.

**Figure 7.** Simulated gain (*H*-plane) for different antenna/phantom distances.



**Table 1.** Antenna gain and radiation efficiency for different antenna/phantom distances.

Antenna position	Gain [dBi] (@ 60 GHz)		Efficiency [%](@ 60 GHz)
	Simulated	Measured	Simulated
Free space	12.1	11.8	92.2
$h = 5.6$ mm	15.1	15.2	75.2
$h = 2$ mm	13.6	13.6	68.2

Table 2 summarizes the numerical results of the absorbed power and peak SAR averaged over 1 g of skin for an input power of 10 mW.

**Table 2.** Absorbed power and maximum SAR averaged over 1 g of skin at 60 GHz for an input power of 10 mW.

	Absorbed power [mW]	Peak SAR <sub>1g</sub> [W/kg]
$h = 5.6$ mm	2.4	1.03
$h = 2$ mm	3.2	1.67

The *E*-field distribution is numerically investigated using a rectangular skin-equivalent phantom (Figure 8). The skin complex permittivity in the frequency range 55–65 GHz is described by Debye model [27] with parameters provided in [21] ( $\epsilon^* = 7.98 - j \cdot 10.90$  at 60 GHz). Figure 9 demonstrates the *E*-field distribution in free space and around the phantom. As it can be seen, due to the presence of the phantom, the main radiation direction is tilted by  $10^\circ$  in the *H*-plane (*xz*-plane) (antenna/phantom distance  $h = 5.6$  mm).

**Figure 8.** End-fire antenna on a rectangular skin-equivalent phantom (dimensions are in mm).

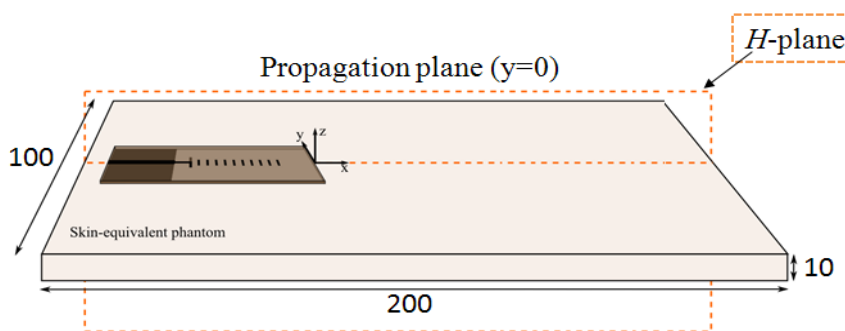
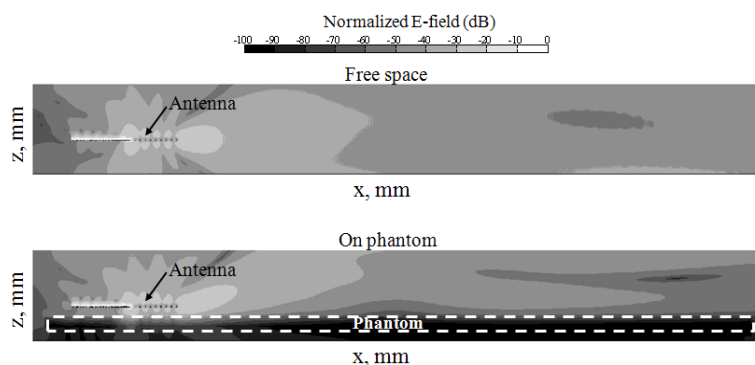


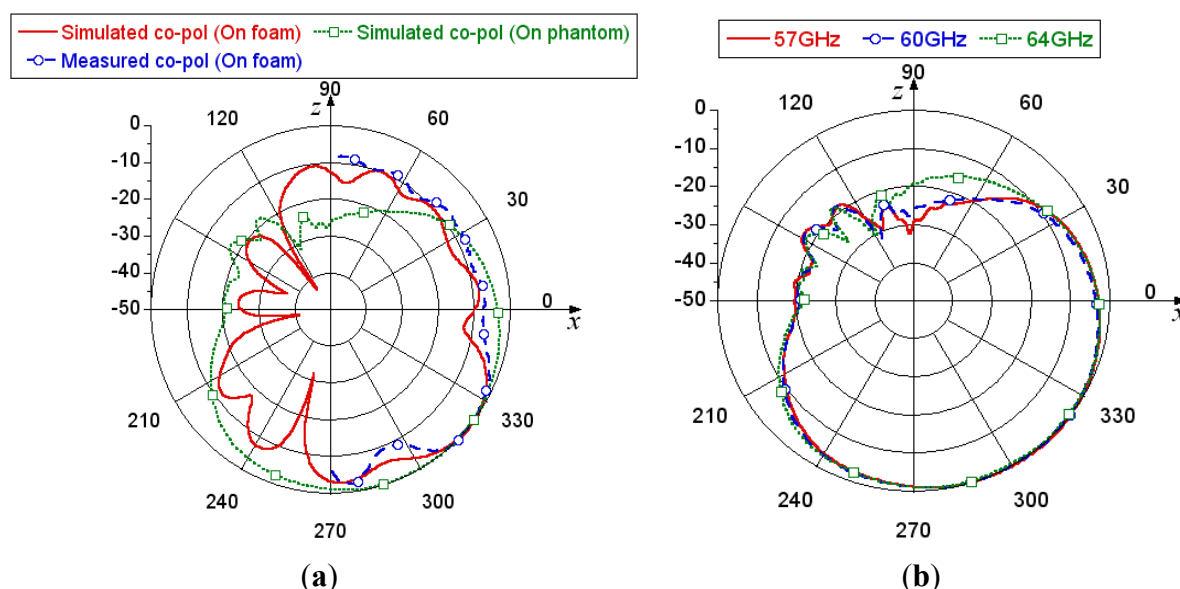
**Figure 9.** *E*-field distribution in free space and around a rectangular skin-equivalent phantom representing a human hand (*xz*-plane) for antenna/phantom distance  $h = 5.6$  mm.



Under bending conditions (Figure 3), a significant effect is noticed on the *H*-plane rather than *E*-plane. Figure 10a shows the measured and simulated radiation pattern in the *H*-plane. When bended, the maximum radiation follows the direction of the directors ( $-46^\circ$  tilt with respect to the flat antenna position in free space). The same effect is noticed at 57 GHz and 64 GHz (Figure 10b). In *E*-plane the angular width (3 dB) increases at  $60^\circ$  for the bent antenna with respect to  $30^\circ$  of the flat antenna position.

As far as the gain is concerned, the measured 11.1 dBi gain is in good agreement with the simulated 11.0 dBi gain. Compared with the free space case, a drop of 0.7 dB is observed during the measurements.

**Figure 10.** (a) *H*-plane (*xz*-plane) radiation pattern of the bent antenna at 60 GHz mounted on a semi-cylindrical foam and skin-equivalent phantom ( $R = 15$  mm); (b) *H*-plane radiation pattern of the bent antenna computed at 57–60–64 GHz mounted on a semi-cylindrical skin-equivalent phantom ( $R = 15$  mm).

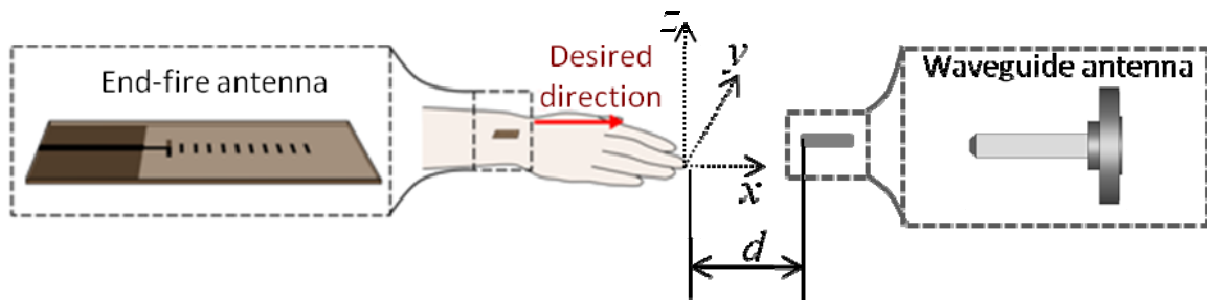


The data presented above demonstrate that when the antenna is mounted on a phantom and/or bended its performances remain satisfactory in terms of reflection coefficient, radiation pattern and efficiency.

### 3. On to off Body Propagation

In this section, a specific communication scenario is considered where the wearable end-fire antenna is placed on a wrist and communicates toward the hand direction with an antenna integrated in an off-body transceiver placed at 5 cm in front of the hand (Figure 11). In practice, the antenna could be integrated in a wristwatch, bracelet, or gloves. To the best of our knowledge, such a high-data-rate exchange scenario has never been investigated so far at millimeter waves.

**Figure 11.** Wearable antenna position on a human hand and waveguide antenna placed in front of the hand as an off-body transceiver.



The propagation for the communication scenario shown in Figure 11 is investigated in terms of path gain (Figure 12). The latter is measured using a Rohde & Schwarz® ZVA67 VNA. Both wearable antenna and waveguide are connected to the VNA ports through 80 cm-long semi-rigid coaxial cables. The waveguide is connected using a waveguide-to-coaxial cable adaptor. Losses in cables and adaptor are taken into account through a full 2-port calibration. The waveguide is fixed at a distance  $d = 5$  cm in front of a phantom and moved in the  $yz$ -plane (from  $-10$  cm to  $10$  cm along  $y$ -axis and from  $0$  cm to  $4$  cm along  $z$ -axis). For these measurements, in addition to the rectangular phantom, we also used a phantom with a realistic hand shape (23 cm length, 2.5 cm height, and 10 cm width). As expected, the maximum path gain is obtained when the waveguide antenna is at a height of about 3–4 cm with respect to the wearable antenna (height corresponding to a  $10^\circ$  tilt in the  $H$ -plane). Higher path gain values are noted for the waveguide position on the  $y$ -axis between  $-5$  cm and  $5$  cm, interval, which corresponds to the angular width of about  $30^\circ$ . This is expected since the radiation pattern of wearable antenna on the  $E$ -plane has an angular width (3 dB) of about  $30^\circ$ . These results are consistent with the power flow distribution in the same cutting plane shown in Figure 13. The difference is mainly related to the radiation pattern and polarization of the open-ended waveguide.

**Figure 12.** Path gain distribution for: (a) rectangular and (b) real hand skin-equivalent phantom. Distance between the phantom and waveguide is  $d = 5$  cm.

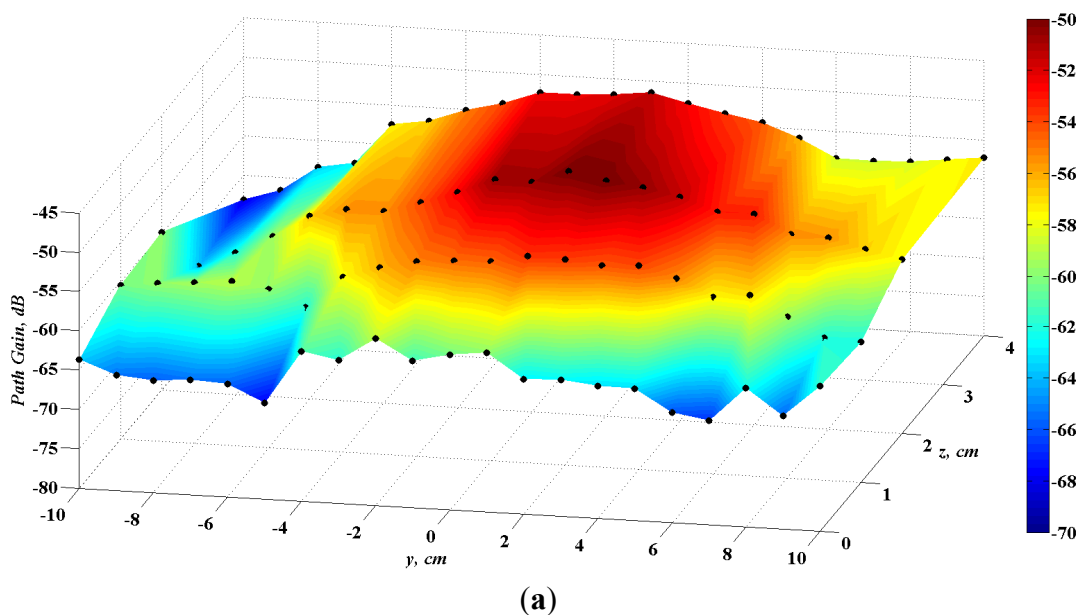


Figure 12. Cont.

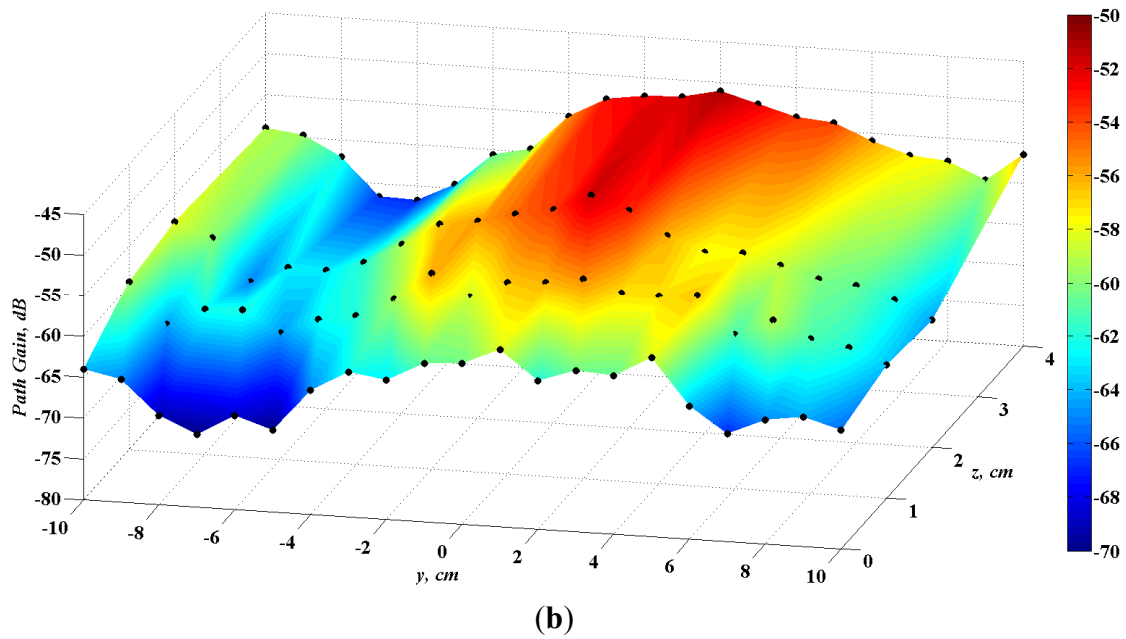
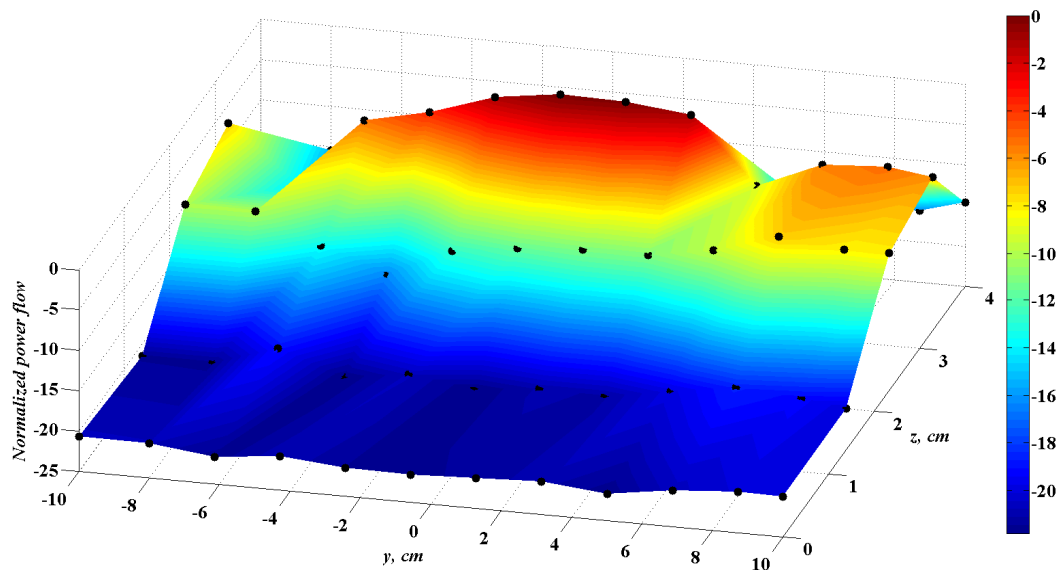


Figure 13. Computed normalized power flow distribution for rectangular skin-equivalent phantom at  $d = 5$  cm.



The data demonstrate that the path gain obtained with the rectangular phantom is similar to the one obtained with the realistic hand model (the maximum deviation is less than 6 dB). This suggests that this propagation path is robust and only slightly sensitive to the hand shape and posture. However, tilting the hand may strongly impact the path gain.

#### 4. Conclusions

In this study, a compact end-fire wearable antenna was characterized in free space, on phantom and under bending conditions. The possibility of its use for an on to off-body communication scenario at 60 GHz was investigated in terms of path gain.

Firstly, the antenna reflection coefficient and radiation patterns were computed and compared with measurements. It was shown that even if under bending conditions the reflection coefficient is affected, it remains below  $-10$  dB. The radiation pattern is mainly affected in the  $H$ -plane with a maximum radiation along the directors ( $-46^\circ$ ), while in the  $E$ -plane an increase of the 3 dB angular width of  $30^\circ$  is observed. It was also demonstrated that when the antenna is placed over a skin-equivalent phantom, both  $E$ - and  $H$ -planes are strongly affected because of reflection from and absorption in the body. In particular, a  $10^\circ$  tilt on the  $H$ -plane radiation pattern is noticed.

Secondly, for the propagation scenario considered in the paper, it was shown that a better propagation occurs when the transmitter is placed in front of the wearable antenna at a height corresponding to the tilt angle noticed in the  $H$ -plane radiation. It was also demonstrated that, for the propagation characterization, a simple rectangular shape phantom can represent a real hand with a difference of less than 6 dB in terms of path gain.

These results suggest that this antenna is a promising candidate for wearable applications within BAN, in particular for high-data-rate transmissions in on/off-body exposure scenarios.

### Acknowledgments

This study was supported by Labex CominLabs (French National Research Agency program “Investing for the Future” ANR-10-LABX-07-01) and Brittany Region under ResCor/BoWI project and by University of Rennes 1. Part of the work was performed using HPC resources from GENCI-IDRIS (grant 2013-050779).

### Conflicts of Interest

The authors declare no conflict of interest.

### References

1. Pellegrini, A; Brizzi, A.; Zhang, L.; Ali, K.; Hao, Y.; Wu, X.; Constantinou, C.C.; Nechayev, Y.; Hall, P.S.; Chahat, N.; *et al.* Antennas and propagation for body centric wireless communications at millimeter wave frequencies: A review. *IEEE Antennas Propag. Mag.* **2013**, *55*, 262–287.
2. Cotton, S.C.; Scanlon, W.G.; Madahar, B.K. Millimeter-wave soldier-to-soldier communications for covert battlefield operations. *IEEE Commun. Mag.* **2009**, *47*, 72–81.
3. Baykas, T.; Sum, C.S.; Lan, Z.; Wang, J.; Rahman, M.A.; Harada, H. IEEE 802.15.3c: The first IEEE wireless standard for data rates over 1 Gb/s. *IEEE Commun. Mag.* **2011**, *49*, 114–121.
4. Cotton, S.C.; Scanlon, W.G.; Hall, P.S. A simulated study of co-channel inter-BAN interference at 2.45 GHz and 60 GHz. In Proceedings of the Wireless Technology Conference (EuWIT), Paris, France, 27–28 September 2010; pp. 61–64.
5. Alipour, S.; Parvaresh, F.; Ghajari, H. Propagation characteristics for a 60 GHz wireless body area network (WBAN). In Proceedings of the Military Communications Conference, San Jose, CA, USA, 31 October 2010–3 November 2010; pp. 719–723.
6. Chahat, N.; Zhadobov, M.; Alekseev, S; Sauleau, R. Human skin-equivalent phantom for on-body antenna measurements in the 60-GHz band. *Electron. Lett.* **2012**, *48*, 67–68.

7. Chahat, N.; Valerio, G.; Zhadobov, M.; Sauleau, R. On-body propagation at 60 GHz. *IEEE Trans. Antennas Propag.* **2013**, *61*, 1876–1888.
8. Guraliuc, A.R.; Zhadobov, M.; Valerio, G.; Chahat, N.; Sauleau, R. Effect of textile on the propagation along the body at 60 GHz. *IEEE Trans. Antennas Propag.* **2014**, *62*, 1489–1494.
9. Zhadobov, M.; Chahat, N.; Sauleau, R.; Le Quément, C.; Le Dréan, Y. Millimeter-wave interactions with the human body: State of knowledge and recent advances. *Int. J. Microw. Wirel. Technol.* **2011**, *3*, 237–247.
10. Wu, X.; Akhoondzadeh-Asl, L.; Wang, Z.; Hall, P.S. Novel Yagi-Uda antennas for on-body communication at 60 GHz. In Proceedings of the Antennas and Propagation Conference (LAPC), Loughborough, UK, 8–9 November 2010; pp. 153–156.
11. Wu, X.; Akhoondzadeh-Asl, L.; Hall, P.S. Printed Yagi-Uda array for on-body communication channels at 60 GHz. *Microw. Opt. Technol. Lett.* **2011**, *53*, 2728–2730.
12. Chahat, N.; Zhadobov, M.; Sauleau, R. Wearable textile patch antenna for BAN at 60 GHz. In Proceedings of the 7th European Conference on Antennas and Propagation (EuCAP), Gothenburg, Sweden, 8–12 April 2013; pp. 209–211.
13. Chahat, N.; Zhadobov, M.; Le Coq, L.; Sauleau, R. Wearable end-fire textile antenna for on-body communications at 60 GHz. *IEEE Antennas Wirel. Propag. Lett.* **2012**, *11*, 799–802.
14. Chahat, N.; Leduc, C.; Zhadobov, M.; Sauleau, R. Antennas and interaction with the body for body-centric wireless communications at millimeter-waves. In Proceedings of the 7th European Conference on Antennas and Propagation (EuCAP), Gothenburg, Sweden, 8–12 April 2013; pp. 757–760.
15. Dey, S.; Saha, N.; Alomainy, A. Design and performance analysis of narrow band textile antenna for three different substrate permittivity materials and bending consequence. In Proceedings of the Antennas and Propagation Conference (LAPC), Loughborough, UK, 8–9 November 2010; pp. 1–5.
16. Hertleer, C.; Tronquo, A.; Rogier, H.; Vallozzi, L.; van Langenhove, L. Aperture-coupled patch antenna for integration into wearable textile systems. *IEEE Antennas Wirel. Propag. Lett.* **2007**, *6*, 392–395.
17. Amaro, N.; Mendes, C.; Pinho, P. Bending effects on a textile microstrip antenna. In Proceedings of the IEEE International Symposium on Antennas and Propagation (APSURSI), Spokane, WA, USA, 3–8 July 2011; pp. 282–285.
18. Locher, I.; Klemm, M.; Kirstein, T.; Troster, G. Design and characterization of purely textile patch antennas. *IEEE Trans. Adv. Packag.* **2006**, *29*, 777–788.
19. Bai, Q.; Langley, R. Crumpling of PIFA textile antenna. *IEEE Trans. Antennas Propag.* **2012**, *60*, 63–70.
20. Zhu, S.; Langley, R. Dual-band wearable textile antenna on an EBG substrate. *IEEE Trans. Antennas Propag.* **2009**, *57*, 926–935.
21. Chahat, N.; Zhadobov, M.; Sauleau, R. Broadband tissue-equivalent phantom for BAN applications at millimeter waves. *IEEE Microw. Theory Technol.* **2012**, *60*, 2259–2266.
22. Wong, K.L.; Lin, C.I. Characteristics of a 2.4-GHz compact shorted patch antenna in close proximity to a lossy medium. *Microw. Opt. Technol. Lett.* **2005**, *45*, 480–483.

23. Hall, P.S.; Hao, Y.; Nechayev, Y.I.; Alomainy, A.; Constantinou, C.C.; Parini, C.; Kamarudin, M.R.; Salim, T.Z.; Hee, D.T.M.; Dubruvka, R.; *et al.* Antennas and propagation for on-body communication systems. *IEEE Antennas Propag. Mag.* **2007**, *49*, 41–58.
24. Chahat, N.; Zhadobov, M.; Sauleau, R.; Ito, K. A compact UWB antenna for on-body applications. *IEEE Trans. Antennas Propag.* **2011**, *59*, 1123–1131.
25. Khan, M.M.; Alomainy, A.; Hao, Y. Dual band and diverse radiation pattern antenna for power efficient and reliable on-body and off-body communications for healthcare applications. In Proceedings of the IEEE International Symposium on Antennas and Propagation (APSURSI), Spokane, WA, USA, 3–8 July 2011; 396–399.
26. Islam, M.R.; Chamok, N.H.; Ali, M. Switched parasitic dipole antenna array for high-data-rate body-worn wireless applications. *IEEE Antennas Wirel. Propag. Lett.* **2012**, *6*, 693–696.
27. Gabriel, S.; Lau, W.; Gabriel, C. The dielectric properties of biological tissues: III. Parametric models for the dielectric spectrum of tissues. *Phys. Med. Biol.* **1996**, *41*, 2271–2293.

© 2014 by the authors; licensee MDPI, Basel, Switzerland. This article is an open access article distributed under the terms and conditions of the Creative Commons Attribution license (<http://creativecommons.org/licenses/by/3.0/>).